Tuning the orientation of the top-facets of GaN nanowires in molecular beam epitaxy by thermal decomposition

T. Auzelle,[1,*] G. Calabrese,[1] and S. Fernández-Garrido[1,2,†]

[1]*Paul-Drude-Institut für Festkörperelektronik, Leibniz-Institut im Forschungsverbund Berlin e. V., Hausvogteiplatz 5–7, 10117 Berlin, Germany*

[2]*Grupo de Electrónica y Semiconductores, Departamento de Física Aplicada, Universidad Autónoma de Madrid, Calle Francisco Tomás y Valiente 7, 28049 Madrid, Spain*

(Received 24 September 2018; published 9 January 2019)

In this work, we demonstrate the possibility of controlling the orientation of the top-facets of GaN nanowires grown by plasma-assisted molecular beam epitaxy by means of an *in situ* thermal treatment at temperatures in the 800–910 °C range, at which the material decomposes with a non-negligible rate. Depending on whether the process is carried out under vacuum or active nitrogen exposure, the nanowires can develop either $\{1\bar{1}0\bar{2}\}$ or $\{1\bar{1}0\bar{8}\}$ semipolar top-facets. The shape transformation is reversible; namely, the original $(000\bar{1})$ polar facets of as-grown nanowires can be recovered after further GaN growth. Using reflection high-energy electron diffraction, the reshaping process is monitored *in vivo* by tracking the formation and subsequent evolution of chevrons in the diffraction pattern. This analysis reveals that the reshaping takes place after a certain delay time that can last up to several tens of minutes. It also evidences that the shape transformation is not abrupt; instead there is a continuous evolution from high- to low-index semipolar facets. We observe energy barriers higher than 3 eV along the reshaping path toward the $\{1\bar{1}0\bar{2}\}$ top-facets. The formation of $\{1\bar{1}0\bar{8}\}$ top-facets is assigned to an intermediate energy minimum along the reshaping path where the system freezes in the presence of active nitrogen. A change in the Ga chemical potential at the nanowire tip is proposed as the trigger for the reshaping, a process that could be either thermodynamically or kinetically driven. The formation of semipolar facets after thermal decomposition is also observed for GaN$(000\bar{1})$ layers, demonstrating that the reshaping process is not related to the peculiar nanowire morphology. This unprecedented ability to form semipolar facets at the tip of N-polar GaN nanowires may pave the way for the fabrication of semipolar axial nanowire heterostructures along the $[000\bar{1}]$ direction.

DOI: 10.1103/PhysRevMaterials.3.013402

I. INTRODUCTION

The thermodynamically stable configuration of group-III nitride compound semiconductors is the wurtzite crystal structure. GaN is thus a polar material characterized by a strong spatial anisotropy in its chemical, structural, and optical properties. Hence, accessing crystal orientations departing from the traditional (0001) can be awarded by dramatic changes in the basic surface properties [1] as well as in the optoelectronic behavior of overgrown heterostructures [2,3]. Various strategies have been devised to synthesize GaN along unconventional orientations, including: heteroepitaxy on novel substrates and homoepitaxy on either three-dimensionally structured GaN films or freestanding GaN layers sliced and polished according to the desired orientation [4].

Within this framework, GaN nanowires are of interest since they feature well-defined and nonequivalent top and sidewall facets [5–8]. Consequently, the properties of axial and radial group-III nitride nanowire heterostructures are fundamentally different. In addition, nanowires benefit from a number of assets, such as a large tolerance to lattice mismatched substrates and the possibility of relaxing strain through elastic deformation [9], which makes them attractive for the fabrication of nanoscale devices. Regardless of the epitaxial technique and growth approach, GaN nanowires typically elongate along either the [0001] or $[000\bar{1}]$ directions, which are known as Ga- and N-polar orientations, respectively [10]. So far, as-grown GaN nanowires invariably exhibit nonpolar $\{1\bar{1}00\}$ sidewall facets [11]. The observed shape of the nanowire tips depends, however, on whether the nanowires are Ga- or N-polar. In the Ga-polar case, the nanowires have a pencil-like shape terminated by semipolar $\{1\bar{1}02\}$ top-facets [12,13]. In the N-polar case, the nanowires have the shape of a hexagonal prism with a flat $(000\bar{1})$ facet at the top [14–16]. These morphologies compare well with the Wulff construction of GaN [17], suggesting a thermodynamic control of the nanowire shape. In this context, finding growth conditions that could enable the tuning of the nanowire morphology by forcing the appearance of new facets is of twofold interest: first to enable the synthesis of novel nanowire heterostructures, and second to challenge the picture of thermodynamically controlled GaN facets.

In this work, with the aim of achieving an unprecedented degree of control on the shape of GaN nanowires, we investigate the stability of the nanowire facets in vacuum and under active N exposure at temperatures for which GaN is

*auzelle@pdi-berlin.de
†sergio.fernandezg@uam.es

thermodynamically unstable against thermal decomposition. The ability to form no previously observed semipolar top-facets as a result of a well-controlled thermal decomposition process is demonstrated by *in situ* and *ex situ* analysis of treated nanowire ensembles. The temporal evolution of the nanowire top-facets is further scrutinized to elucidate the conditions that trigger the reshaping. A direct correlation between the GaN decomposition rate and the onset of the reshaping process is evidenced. Finally, the use of a thermal treatment as a means to form semipolar facets is also extended to the case of GaN(000$\bar{1}$) films.

II. EXPERIMENTAL DETAILS

The GaN nanowire ensembles studied here are prepared in a plasma-assisted molecular beam epitaxy (PA-MBE) system equipped with an effusion cell to provide Ga and a radio-frequency plasma source to generate active N. The Ga and N fluxes are calibrated in units of monolayers per second (ML/s), where 1 ML corresponds to 1.14×10^{15} Ga and N pairs cm^{-2} [18]. The synthesis of the GaN nanowires is carried out on Si(111) substrates and relies on a self-assembled growth approach [19]. Following an *in situ* thermal deoxidation of the Si substrate, nanowires are either grown on the bare Si surface or on a 1–10 nm thick AlN buffer layer prepared as described by Largeau *et al.* [20]. We typically use a substrate growth temperature of 830–860 °C, a substrate rotation speed of 2 rpm, a N flux of 1–1.6 ML/s and a III/V ratio of 0.2–0.3 for both the nucleation and growth of nanowires. The substrate temperature is measured by an optical pyrometer operating at 920 nm and calibrated against the appearance of the 7×7-Si(111) surface reconstruction occurring at 860 °C [21]. Once the nanowires reach a length of 0.5–1.5 μm, the growth is interrupted by shuttering the Ga and N cells. The reshaping of the nanowire top-facets is eventually investigated in the temperature range of 800–910 °C, where the material is known to be unstable against thermal decomposition [22,23]. The substrate temperature is changed at a typical rate of 0.5 °C/min. For reshaping under active N exposure, the nanowire ensemble is exposed to a 1–1.6 ML/s N flux produced by the plasma cell. For reshaping under vacuum, the N plasma cell is shuttered but not turned off meaning that a leaking N flux exists.

According to the literature, the nanowire top-facets are expected to be of the $\{hkl\bar{n}\}_{n>0}$ family (i.e., N-polar) with the possible presence of Ga-polar inversion domains, no matter whether they are grown on bare or AlN-buffered Si(111) [10].

The nanowire thermal decomposition is monitored inside the PA-MBE system by line-of-sight quadrupole mass spectrometry (QMS) and reflection high-energy electron diffraction (RHEED). QMS is used to assess the decomposition rate of GaN by measuring the desorbing Ga^{69} signal [23–26]. The QMS response is calibrated in GaN-equivalent growth rate units of ML/s, as described in Ref. [25]. RHEED is used to detect the appearance of new top-facets. The electron gun is operated using a 20 kV acceleration voltage. Custom PYTHON routines are employed for the processing of RHEED patterns, as further described below. The nanowire ensembles are also *ex situ* analyzed by cross-sectional scanning electron microscopy (SEM) using a field-emission microscope.

The N-polar GaN layers investigated at the end of this work are prepared in a PA-MBE system similar to that of the GaN nanowires. As substrates, we use in this case 350 μm thick freestanding GaN(000$\bar{1}$) layers with a 0.35 deg miscut toward the [1$\bar{1}$00] direction and a nominal dislocation density below 5×10^6 cm^{-3} (purchased from Suzhou Nanowin Science and Technology). To preserve the smoothness of the as-received substrates, our GaN layers are prepared using Ga-rich growth conditions [27].

III. RESULTS

A. Formation of semipolar GaN nanowire top-facets

First, a series of three GaN nanowire ensembles are grown at 830 °C on AlN-buffered Si. Compared to the case of direct nucleation on bare Si, the AlN buffer is beneficial at decreasing the tilt dispersion within the nanowire ensemble, which significantly sharpens the GaN-related RHEED patterns. The improved orientation likely stems from the absence of the amorphous Si_xN_y interlayer [28] formed when GaN nanowires are directly grown on Si [29]. Distinct procedures are followed to end the growth of the three different nanowire ensembles:

(1) *As-grown*: At the end of the growth both the N and Ga fluxes are shuttered. Then, the substrate temperature is decreased to 100 °C.

(2) *N-exposed*: At the end of the growth the Ga flux is shuttered and the nanowires are exposed to an active N flux of 1.2 ML/s. The substrate temperature is subsequently increased to 850 °C for 10 min. Finally, the sample is cooled down to 100 °C at which the N flux is shuttered.

(3) *Vacuum-exposed*: At the end of the growth both the N and Ga fluxes are shuttered. Afterwards, the substrate temperature is increased to 870 °C for 30 min. Then, the sample is cooled down to 100 °C.

For all samples, once the substrate reaches a temperature below 400 °C, we record the GaN RHEED patterns along both the [11$\bar{2}$0] and [1$\bar{1}$00] azimuths. The patterns exhibit the diffraction spots expected for 3D GaN nanostructures, with the addition of faint chevrons as shown in the insets of Fig. 1. The chevrons emanate from the spots and extend towards the shadow edge. The appearance of chevrons is attributed to electron diffraction on facets and electron transmission through crystal edges [30–32]. In the latter case, the refraction induces a deviation of the transmitted beam toward the shadow edge, with a spread in the refraction angle caused by the small size of the diffracting object [33]. In both cases, the two branches of the chevron (from now on directly referred as chevrons) are perpendicular to the contour of the diffracting object projected on the azimuthal plane, allowing us to retrieve the object morphology [33–39]. Using a custom routine, we extract the angular profiles of the RHEED intensity around selected GaN diffraction spots for the three samples under scrutiny, which are shown in Figs. 1(a)–1(f). Due to the large nanowire number density ($>4 \times 10^9$ cm^{-2}), diffraction from the GaN parasitic layer that develops in between nanowires is ruled out because the 20 keV electrons would have to travel through more than 2 μm of GaN, which largely exceeds their ∼5 nm inelastic mean-free path [40]. Consequently, the analysis of

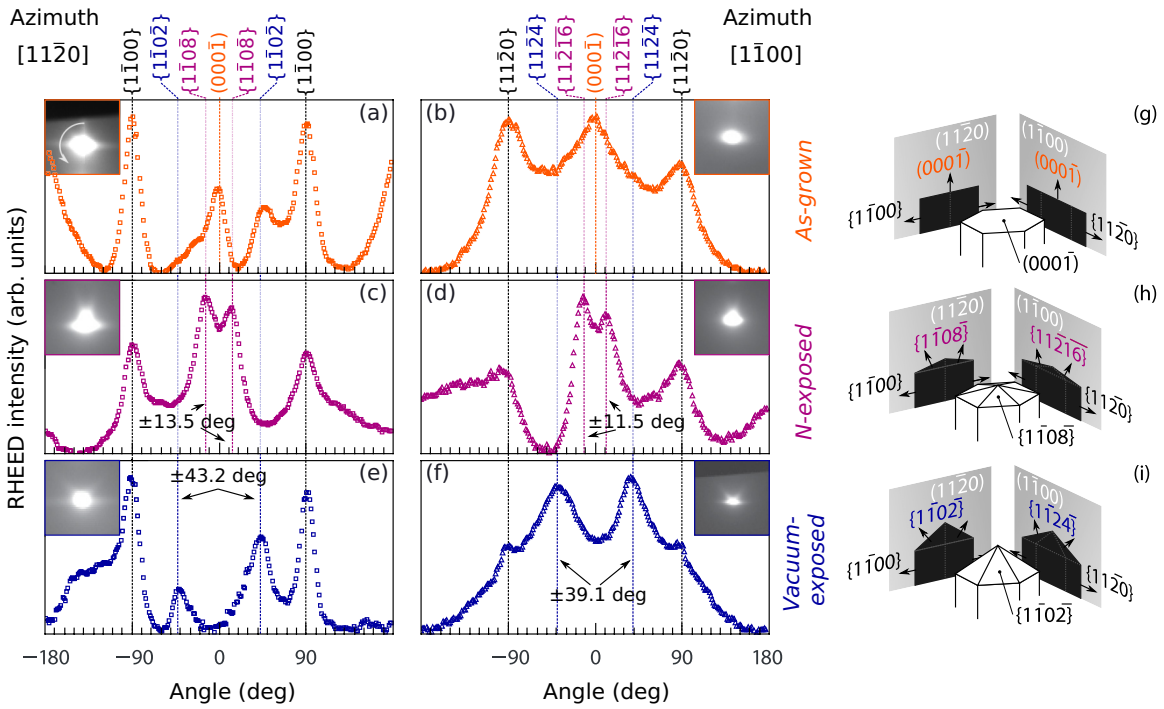

FIG. 1. (a)–(f) Angular RHEED intensity profiles around selected GaN diffraction spots of patterns recorded along the [1$\bar{1}$20] and [1$\bar{1}$00] azimuths (as indicated at the top of the figures) of (a) and (b) as-grown, (c) and (d) N-exposed, and (e) and (f) vacuum-exposed nanowire ensembles. The raw pictures of the corresponding diffraction spots are shown in the respective insets. The 0 deg direction is parallel to the [0001] direction in the GaN reciprocal space (perpendicular to the shadow edge and vertical in the images) and the rotation direction is counterclockwise, as sketched in the inset of (a). GaN planes, for which the observed chevrons are perpendicular, are indicated on the graphs by dashed lines (the indexes for those facets are shown at the top). (g)–(i) Schematic of the average nanowire top-facets and their projection on the (11$\bar{2}$0) and (1$\bar{1}$00) azimuthal planes as deduced from the chevron orientation of (g) as-grown, (h) N-exposed, and (i) vacuum-exposed nanowire ensembles. Arrows in the azimuthal planes are normal to the labeled planes.

the chevron angles can be used to gain, *in situ*, insights into the orientation of the nanowire top-facets.

For the three nanowire ensembles investigated here, we observe different chevrons along the [11$\bar{2}$0] and [1$\bar{1}$00] azimuths [Figs. 1(a)–1(f)]. The extracted angle of the chevrons is used to reconstruct the projection of the average nanowire top-facets on the (11$\bar{2}$0) and (1$\bar{1}$00) azimuthal planes and eventually provides the average nanowire top-facet orientation, as sketched in Figs. 1(g)–1(i). Chevrons parallel to the shadow edge (at ±90 deg), attributed to diffraction at the nanowire sidewalls, are observed in the three samples. In contrast, inclined chevrons, associated with the nanowire top-facets, are seen with different angles depending on the specific sample treatment, namely:

(i) The as-grown nanowire ensemble exhibits chevrons perpendicular to the (000$\bar{1}$) plane [see Figs. 1(a) and 1(b)]. As depicted in Fig. 1(g), they are the signature of (000$\bar{1}$) top-facets. In addition, there are also chevrons perpendicular to the {1$\bar{1}$0$\bar{2}$} planes, as shown in Fig. 1(b). The latter suggest the additional presence of {1$\bar{1}$0$\bar{2}$} facets.

(ii) The N-exposed nanowire ensemble exhibits chevrons perpendicular to the {1$\bar{1}$0$\bar{8}$} and {1 1 $\bar{2}$ 1$\bar{6}$} planes along the [11$\bar{2}$0] and [1$\bar{1}$00] azimuths, respectively [see Figs. 1(c) and 1(d)]. These chevrons indicate the existence of {1$\bar{1}$0$\bar{8}$} semipolar facets, as sketched in Fig. 1(h). Indeed, the chevrons perpendicular to the {1 1 $\bar{2}$ 1$\bar{6}$} facets are attributed to refraction at the edges delimiting the {1$\bar{1}$0$\bar{8}$} facets. Interestingly, in this case we do not observe chevrons perpendicular to the (000$\bar{1}$) plane. Consequently, we rule out the presence of (000$\bar{1}$) top-facets.

(iii) The vacuum-exposed nanowire ensemble exhibits chevrons perpendicular to the {1$\bar{1}$0$\bar{2}$} and {11$\bar{2}\bar{4}$} planes along the [11$\bar{2}$0] and [1$\bar{1}$00] azimuths, respectively [see Figs. 1(e) and 1(f)]. Both types of chevrons are assigned to the presence of {1$\bar{1}$0$\bar{2}$} semipolar facets as shown in Fig. 1(i). Once again, the lack of chevrons perpendicular to the (000$\bar{1}$) plane indicates the absence of (000$\bar{1}$) top-facets.

In order to confirm the presence of the nanowire facets identified *in situ* by RHEED, the three samples are further analyzed *ex situ* by SEM. The specimens used for the cross-sectional inspection at the scanning electron microscope are obtained by cleaving the samples along the ⟨110⟩ direction of the Si substrate. Because of the well-defined in-plane epitaxial relationship of the nanowires with respect to the Si substrate, $[1\bar{1}00]_{GaN} \parallel [1\bar{1}0]_{Si}$ [11], in the scanning electron micrograph we observe the projection of the nanowire shapes on the (1$\bar{1}$00) plane. Side-view micrographs of the tip of representative nanowires are presented in Figs. 2(i)–2(iv). In line with the results obtained by RHEED, the nanowire tips exhibit different shapes depending on the final sample treatment. For the three samples under scrutiny, the corresponding histograms of the projected top-facet angles, derived from the analysis of about 100 nanowires per sample, are shown in Fig. 2. The theoretical positions of the projected angles of

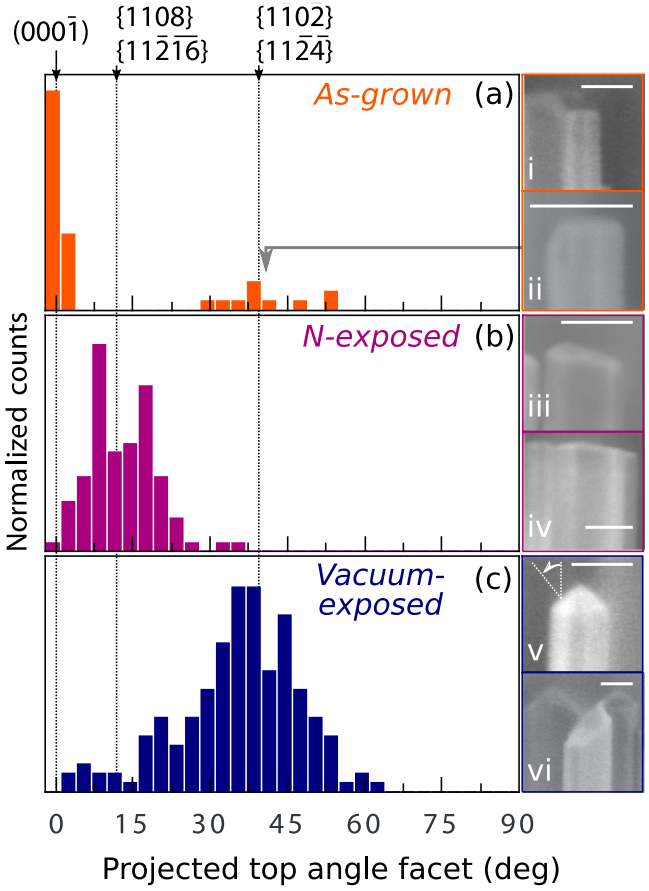

FIG. 2. Histograms of the nanowire top-facet angles projected on the (1$\bar{1}$00) plane for the (a) as-grown, (b) N-exposed. and (c) vacuum-exposed nanowire ensembles. For each ensemble, we analyze about 100 nanowires. The arrows indicate, for a selection of GaN facets, the theoretical projected facet angles. The insets (i)–(vi) are [1$\bar{1}$00] side-view scanning electron micrographs of typical nanowires from the corresponding ensembles. The extraction of the projected top-facet angles from the scanning electron micrographs is exemplified in (v). The scale bars in (i)–(vi) represent 50 nm.

the top-facets detected by RHEED are indicated by vertical arrows in the histograms. As can be observed, the results obtained by RHEED and SEM are in excellent agreement. We note that the top-facet angle distributions for the N- and vacuum-exposed nanowires are rather broad (±10 deg), indicating that not all nanowire tips have an identical shape. In the case of the as-grown sample, a minority of nanowires exhibit semipolar top-facets, as expected according to the observation of chevrons perpendicular to the {1$\bar{1}$0$\bar{2}$} planes in the RHEED pattern recorded along the [11$\bar{2}$0] azimuth [Fig. 1(a)]. Interestingly, the {1$\bar{1}$0$\bar{2}$} facets are systematically paired with a (000$\bar{1}$) facet [see Fig. 2(ii)]. This morphology is in close agreement with the results of Galopin *et al.* [41] who pictured GaN nanowire top-facets at various times during growth, using AlN markers and *ex situ* transmission electron microscopy.

The results presented so far demonstrate that, on average, as-grown nanowires have polar (000$\bar{1}$) top-facets, whereas N- and vacuum-exposed nanowires develop, respectively, semipolar {1$\bar{1}$0$\bar{8}$} and {1$\bar{1}$0$\bar{2}$} facets at their tips. The shape of the GaN nanowires can thus be modified *in situ* upon the growth process by either N or vacuum exposure at elevated temperatures, where the material is known to be unstable against thermal decomposition [22,23].

B. Temporal evolution of the nanowire reshaping

The visualization of RHEED chevrons can be advantageously used to track *in vivo* the evolution of the nanowire top-facets during the reshaping process as well as to systematically investigate how the shape transformation depends on different parameters. With this purpose in mind, several GaN nanowire ensembles are grown again on AlN-buffered Si substrates and subsequently subjected to various N-exposure steps (Ga flux shuttered and N flux open) and vacuum-exposure steps (Ga and N fluxes shuttered) carried out at a fixed substrate temperature. In general, the experiments with a given nanowire ensemble end once the contrast of the chevrons becomes too weak, mainly due to an increasing tilt dispersion assigned to nanowire bundling [42]. During the reshaping experiments, RHEED movies are acquired along a certain azimuth. Then, we extract angular intensity profiles around selected GaN diffraction spots from movie frames. We note that the chevrons' intensity at high substrate temperature is weaker than for the case of Fig. 1. To enhance their contrast, the contribution from the {1$\bar{1}$00} diffraction streaks is removed from each angular intensity profile using a Gaussian fit. It follows that the intensity profile of the chevrons often appears asymmetric and with overestimated chevron angles. Therefore, in the following, we only discuss qualitative variations of the chevron angles and the top-facets indexes are extrapolated from the analysis presented in Sec. III A.

Figure 3(a) presents exemplary maps of the angular RHEED intensity profile for two different experiments. In the experiment labeled as i, after the formation of the GaN nanowires, the ensemble is subjected to a series of consecutive steps at 870 °C, namely, N exposure, vacuum exposure, GaN growth, and vacuum exposure. The temporal evolution of the angular RHEED intensity profile evidences variations of the average nanowire shape under either N or vacuum exposure. These steps, respectively, stabilize high-index and low-index semipolar top-facets, as already found for N- and vacuum-exposed nanowire ensembles. It confirms that N and vacuum exposures induce the nanowire reshaping by respectively stabilizing {1$\bar{1}$0$\bar{8}$} and {1$\bar{1}$0$\bar{2}$} facets. Interestingly, after the first vacuum-exposure step, the initial (000$\bar{1}$) top-facets are seen to recover as soon as GaN growth is resumed. The nanowire reshaping is thus a reversible process. In the experiment labeled as ii, we show the evolution of the angular RHEED intensity profile at 845 °C for a nanowire ensemble subjected to N-exposure, vacuum-exposure, N-exposure, and GaN-growth steps. The first N exposure initiates a reshaping but not the second one. This suggests that the reshaping only proceeds from high- to low-index semipolar facets. Nevertheless, the (000$\bar{1}$) top-facet is recovered immediately after initiating GaN growth.

We only observe nanowire reshaping as those illustrated in Fig. 3(a) at substrate temperatures above ∼800 °C.

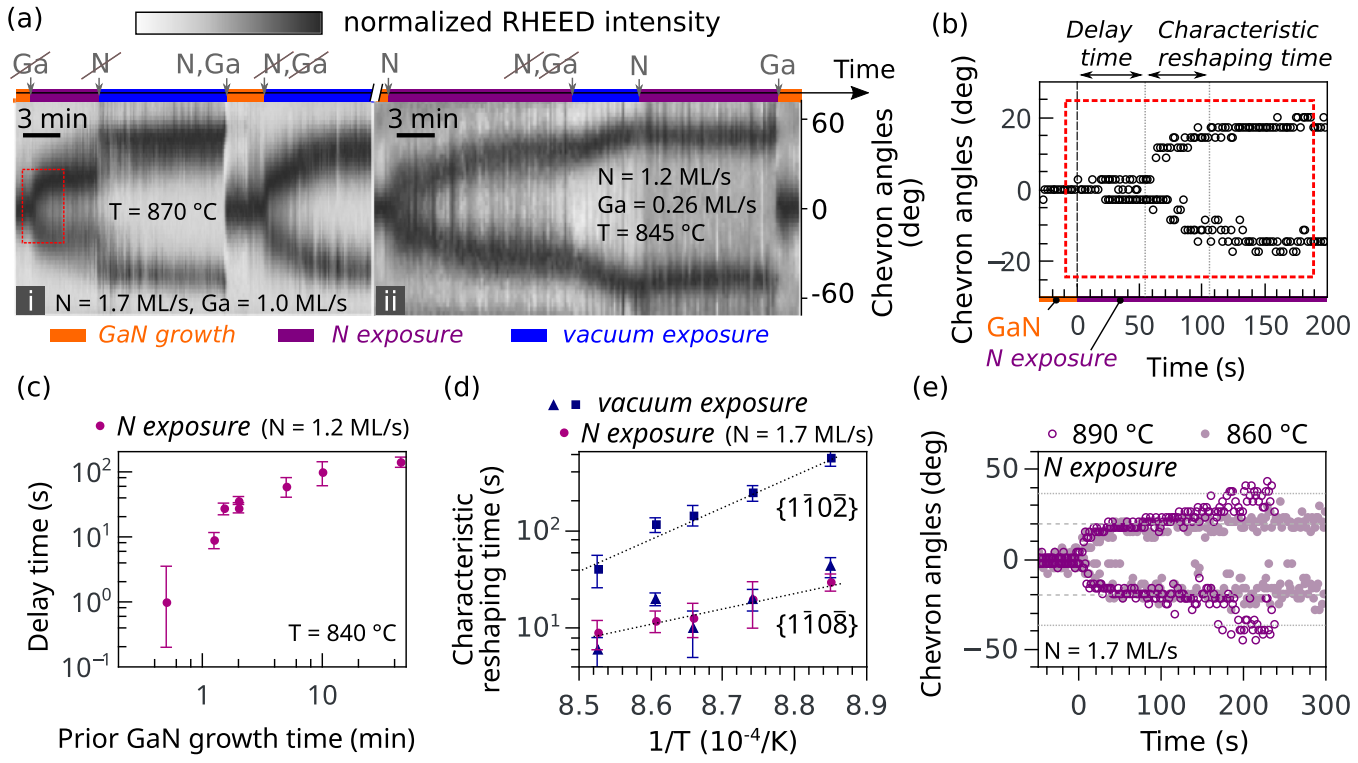

FIG. 3. (a) Intensity map illustrating the temporal evolution of angular RHEED intensity profiles recorded along the [11$\bar{2}$0] azimuth after various Ga and N shutter sequences for two different experiments labeled as i and ii. The opening/closing events of the Ga and N shutters are shown by arrows at the top of the time line. The nanowire ensembles are different in i and ii. (b) Average chevron angles extracted from the N-exposure step highlighted by a red rectangle in (a) as a function of the time (the Ga shutter is shuttered at $t = 0$ s). (c) Logarithmic plot of the delay time observed prior to the reshaping of GaN nanowires under N exposure as a function of the GaN growth duration prior to shuttering the Ga cell. (d) Arrhenius representation of the temperature dependence of the characteristic nanowire reshaping time toward {1$\bar{1}$08} top-facets measured for N exposure and toward {1$\bar{1}$08} and {1$\bar{1}$02} top-facets measured for vacuum exposure. The dotted lines are fits yielding an activation energy of 3.3 ± 0.3 and 6.6 ± 0.6 eV for the respective formation of {1$\bar{1}$08} and {1$\bar{1}$02} top-facets. (e) Average chevron angles for two N-exposure steps performed at a substrate temperature of 860 and 890 °C for the same nanowire ensemble. The time origin is set once the reshaping sets in. The N exposure at 890 °C is interrupted after 250 s. This is the reason why no more data points are shown beyond this time for the experiment performed at 890 °C.

Besides the necessity of a minimum substrate temperature, the formation of new facets requires time, typically on the order of several tens of min. This observation is in striking contrast to the almost instantaneous recovery of the (000$\bar{1}$) top-facets upon resuming GaN growth [Fig. 3(a)]. Interestingly, during the reshaping process, there is a continuous change in the angle of the chevrons, no matter whether the nanowires are reshaped under N or vacuum exposure, as can be observed in Fig. 3(a). Since the RHEED beam probes $\sim 10^8$ nanowires, the change in the angle of the chevrons implies a simultaneous reshaping of most nanowires via the formation of high-index semipolar facets. A closer look into the reshaping period is provided in Fig. 3(b), where we plot the time evolution of the average chevron angles after shuttering the Ga cell to initiate the first N-exposure step shown in Fig. 3(a)i (highlighted by a red rectangle). After closing the shutter, we observe two transients:

i. First, a *delay time*. During this time, despite that the Ga shutter is already closed, the reshaping has not yet set in. Note that the ±5 deg dispersion in the chevron angles measured during the delay time is an artifact from the fitting routine and does not correspond to a top-facet reshaping.

ii. Second, a characteristic *reshaping time*. This time describes the period during which the nanowire top-facets continuously evolve until reaching their final orientation.

These two transients are systematically observed during reshaping experiments under N and vacuum exposure (vacuum-exposure experiments are not shown here).

Next, we analyze how the transients are influenced by the GaN growth time prior to the reshaping, and the substrate temperature. To this end, we perform a series of subsequent reshaping experiments on the same nanowire ensemble whose top-facets are systematically reinitialized to their original (000$\bar{1}$) orientation by GaN regrowth. Unexpectedly, the delay time measured for N exposure steadily increases with the time employed to recover the (000$\bar{1}$) facets [see Fig. 3(c)]. The existence of a similar trend has not been investigated for the reshaping under vacuum exposure. The effect of the substrate temperature on the characteristic reshaping times describing the formation of {1$\bar{1}$08} and {1$\bar{1}$02} top-facets under, respectively, N and vacuum exposure is summarized in the Arrhenius plots shown in Fig. 3(d). The characteristic reshaping time related to the intermediate formation of {1$\bar{1}$08} top-facets under vacuum exposure is also included

in Fig. 3(d). In all the cases, the characteristic reshaping times are well described by Arrhenius laws, which evidences the existence of energy barriers along the reshaping path. The obtained activation energy for the formation of $\{1\bar{1}0\bar{8}\}$ top-facets amounts to 3.3 ± 0.3 eV in both cases of N and vacuum exposures. This value is close to the reported apparent activation energy for GaN(0001) decomposition (3.1 eV) [23]. It suggests the requirement of GaN decomposition to enable the nanowire reshaping. An activation energy of 6.6 ± 0.6 eV is extracted for the formation of $\{1\bar{1}0\bar{2}\}$ under vacuum exposure. It evidences the existence of even higher energy barriers along the reshaping path, localized between the intermediate and final $\{1\bar{1}0\bar{8}\}$ and $\{1\bar{1}0\bar{2}\}$ facets, respectively. Nonetheless, this energy barrier of 6.6 ± 0.6 eV is seen to decrease to ~4 eV when decreasing the N flux leaking from the shuttered N cell (not shown here). Therefore, we will not pursue a further quantitative analysis of this energy barrier which clearly depends on the active N background pressure.

While exploring higher substrate temperatures, deviations in the nanowire reshaping under N exposure are observed. As exemplified in Fig. 3(e), the $\{1\bar{1}0\bar{8}\}$ semipolar top-facets newly formed under N exposure at 890 °C are not stable and further evolve after ~3 min into lower-indexed semipolar facets. This is not the case if performing the N exposure at 860 °C. Similarly in Fig. 3(a), the initial N exposure of the experiment ii first results in high-indexed semipolar facets (attributed to $\{1\bar{1}0\bar{8}\}$ facets) which evolve ~5 min later into lower-indexed semipolar facets. Both cases suggest that $\{1\bar{1}0\bar{8}\}$ facets are only kinetically stabilized and constitute an intermediate step within the reshaping path toward lower indexed semipolar top-facets. Their kinetic stabilization would then depend on the substrate temperature and on the flux of active N.

C. Role of thermal decomposition in the reshaping process

The existence of energy barriers higher than 3 eV along the reshaping path suggests that the thermal instability of GaN triggers the process. The rate at which a GaN nanowire ensemble decomposes in a low-pressure environment can be measured *in situ* by QMS [26]. In the present case, however, the GaN(0001) parasitic layer that develops in parallel to the formation of nanowires on AlN-buffered Si [20,28] adds a non-negligible contribution to the GaN decomposition rate inferred from QMS measurements. Thus, in order to investigate the decomposition of GaN during the reshaping process by QMS, additional GaN nanowire ensembles are prepared on bare Si, where the parasitic layer does not form. Besides the measurement of the GaN decomposition rate, we also analyze the formation of semipolar facets *ex situ* by SEM. Note that the large tilt dispersion of the nanowires grown on bare Si [43] prevents the *in situ* analysis by RHEED.

Figure 4(a) presents the temporal evolution of the GaN decomposition rate of a nanowire ensemble annealed in vacuum after growth at 880 °C for 60 min. The time origin is set once the substrate temperature reaches the annealing temperature, i.e., 880 °C. A ~30 min initial transient state in the GaN decomposition rate is observed before reaching a steady state characterized by a monoexponential decay, as the one reported by Zettler *et al.* [26]. To elucidate whether the initial transient correlates with changes in the nanowire shapes, similar GaN nanowire ensembles are prepared and subsequently annealed under identical conditions but for different times, namely, 1, 12, 22, and 32 min. The results derived from their *ex situ* characterization by SEM are summarized in Fig. 4(c) where we present the histograms of the nanowire top-facet angles projected onto the $(1\bar{1}00)$ plane together with representative scanning electron micrographs. As can be observed, semipolar top-facets are seen on all of the nanowires for annealing times of 32 min or more, i.e., once the initial transient state in the QMS signal is over.

To gain further insight into the origin of the transient state observed in the thermal decomposition rate, three additional GaN nanowire ensembles are grown and subsequently annealed for 11 ± 1 min at 840, 900, and 910 °C. The GaN decomposition rate measured for these samples and the one previously prepared at 880 °C are plotted together in Fig. 4(b). Within the timescale of the experiment, we only observe the monoexponential decay in the decomposition rate for the sample prepared at 910 °C. Assuming that the change in the annealing temperature alters the timescale but not the shape of the initial transient state, we deduce that the transient state becomes shorter for increasing annealing temperatures. For instance, the transient state at 880 °C amounts to ~30 min [Fig. 4(a)], whereas it drops to less than 10 min at 910 °C. As for previous experiments, the samples are further analyzed *ex situ* by SEM [Fig. 4(d)]. A majority of semipolar top-facets is seen only in the case of the nanowire ensemble annealed at 910 °C, for which the transient state is (or close to being) over. On the basis of these results, it is clear that the delay time detected prior to the reshaping of the nanowire tips under vacuum exposure is correlated to the transient state observed in the GaN decomposition rate by QMS.

According to Zettler *et al.* [26], the steady state decomposition of GaN nanowires occurs layer-by-layer and is triggered by the removal of Ga and/or N atoms at the edges of the nanowire tips, where the coordination number of the atomic sites reaches its minimum value. The initial transient state in the thermal decomposition rate could then be related to either (i) an enhanced decomposition rate at extended defects formed at the joint boundaries of coalesced nanowires [42,44], or (ii) the time required to induce the nanowire reshaping. In other words, we cannot conclude at this stage whether this transient state is the cause or the consequence of the delay time, but both correlate.

To shine further light on the origin of the delay time, we analyze the length of GaN nanowire ensembles annealed under vacuum exposure at 880 °C for different times. The dependence of the final average nanowire length on the decomposition time is shown in Fig. 4(e). The plot reveals that the nanowires are already shorter than their nominal length before the end of the transient state, occurring after ~30 min. Consequently, GaN nanowires start decomposing from their tips before the shape transformation sets in. The nanowire reshaping is thus not only triggered by thermal decomposition.

At last, we note that in the case of the GaN nanowire ensembles prepared on bare Si, the vacuum exposure times employed in the experiments described above were never long enough to form a majority of nanowires with $\{1\bar{1}0\bar{2}\}$ top-facets. This observation is in contrast to the results

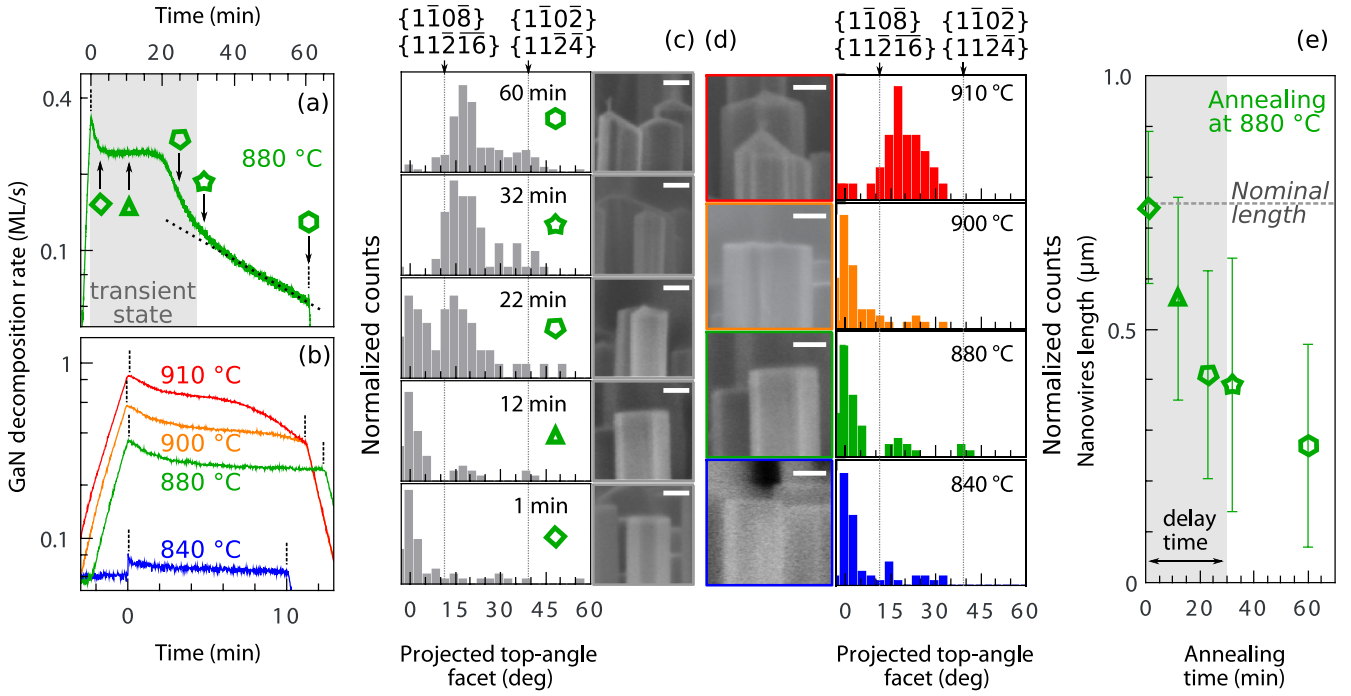

FIG. 4. (a), (b) GaN decomposition rate measured by QMS during the annealing of GaN nanowire ensembles at different temperatures. For each curve, the vertical dashed lines delimit the time frame for which the substrate is maintained at the indicated temperature. The dotted line in (a) illustrates a monoexponential decay as reported by Zettler *et al.* [26] and the gray area depicts the transient state. The polygons in (a) refer to additional nanowire ensembles annealed at 880 °C for shorter times. (c), (d) Histograms of the nanowire top-facet angles projected on the (1$\bar{1}$00) plane for ensembles annealed at (c) 880 °C for different durations, and (d) different temperatures for 11 ± 1 min. To construct each histogram, we analyze about ∼60 nanowires per sample. The insets show side-view scanning electron micrographs of typical nanowires from the respective ensembles. The scale bars in the insets of (c) and (d) represent 50 nm. (e) Average nanowire length of ensembles annealed at 880 °C as a function of the annealing time.

obtained on the nanowire ensembles prepared on the AlN buffer layers, which developed the final {1$\bar{1}$0$\bar{2}$} in shorter times. Since the morphological properties of the nanowire ensembles depend on whether they are grown on bare or AlN-buffered Si, this observation indicates that the reshaping process, and more particularly the reshaping time, are also affected by the diameter and distribution of the GaN nanowires within the ensemble.

D. Formation of semipolar facets in GaN(000$\bar{1}$) layers

To elucidate whether the formation of semipolar facets in GaN nanowires is a direct consequence of their peculiar morphology, we examine next the possible formation of semipolar facets on initially smooth freestanding GaN(000$\bar{1}$) layers. The use of freestanding GaN layers as substrates for this study is primarily intended to benefit from their low density of threading dislocations ($<5 \times 10^6$ cm^{-2}), a choice that allows us to probe GaN surfaces as similar as possible to the initially flat (000$\bar{1}$) top-facets of as-grown nanowires.

A first experiment is performed consisting of decomposing in vacuum a smooth N-polar GaN layer prepared by PA-MBE under Ga-rich growth conditions on a freestanding GaN layer. The effective GaN decomposition is assessed by the observation of a desorbing Ga flux from the substrate by QMS, meaning that the substrate temperature is above 700 °C [23]. As for the experiments with the GaN nanowires, we analyze the final morphology of the GaN layer *in situ* and *ex situ* by RHEED and SEM, respectively. As shown in Figs. 5(a) and 5(b), the appearance of chevrons in the RHEED pattern during the thermal decomposition process reveals the formation of semipolar facets under vacuum exposure. From the analysis of the chevron angles, we deduce that the semipolar facets stabilized under vacuum exposure are {1$\bar{1}$0$\bar{2}$} and {11$\bar{2}$$\bar{3}$} facets. These facets, shown in the scanning electron micrograph of Fig. 5(c), recall those observed at the end of the reshaping process of GaN nanowires in vacuum. We thus conclude that the formation of semipolar facets during vacuum exposure is an intrinsic property of N-polar material and not enabled by the specific nanowire geometry. As for the exact orientation of the stabilized semipolar facets, differences are observed between the layer and nanowire cases, which are tentatively ascribed to the presence of {1$\bar{1}$00} sidewalls in the nanowire case.

Thermal decomposition in vacuum can be seen as the reverse reaction of GaN growth. Hence, it is tempting to compare the facets formed during these two opposite processes. According to the literature, GaN(000$\bar{1}$) growth under Ga-rich conditions leads to the formation of flat and smooth surfaces, whereas N-rich growth is known to result in GaN layers with rough morphologies [27,45]. To examine the roughening induced under N excess, we grow GaN under N-rich conditions on a smooth surface prepared by PA-MBE on a freestanding GaN(000$\bar{1}$) layer. The analysis of the sample by RHEED and SEM, summarized in Figs. 5(d)–5(f), reveals that the roughening of the GaN layer occurring under N-rich

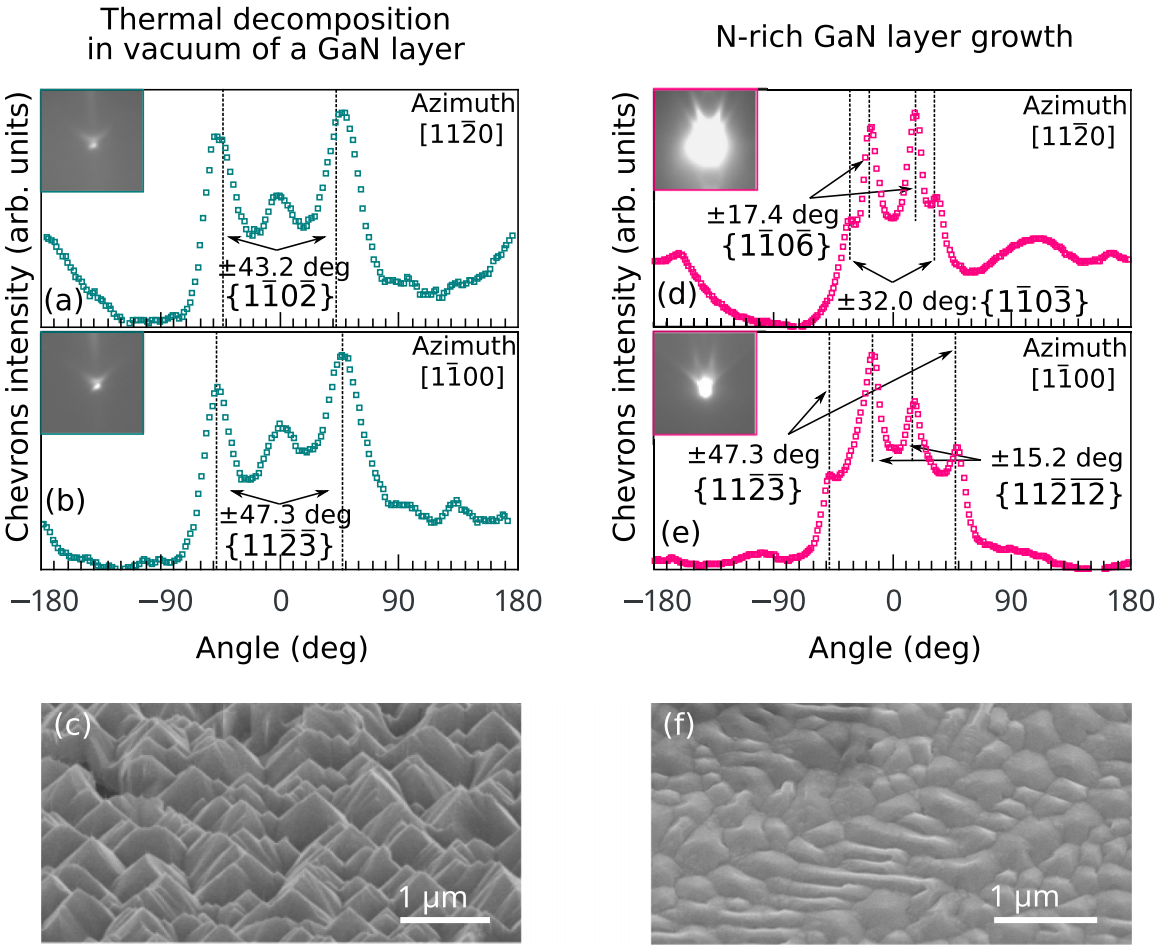

FIG. 5. (a), (b) Angular RHEED intensity profiles around selected GaN diffraction spots recorded along the (a) [11$\bar{2}$0] and (b) [1$\bar{1}$00] azimuths upon the onset of the decomposition process of a GaN(000$\bar{1}$) layer above 700 °C. (c) Bird's eye view scanning electron micrograph of a GaN(000$\bar{1}$) layer thermally decomposed above 700 °C for 180 min. (d), (e) Angular RHEED intensity profiles around selected GaN diffraction spots recorded along the (d) [11$\bar{2}$0] and (e) [1$\bar{1}$00] azimuths after the N-rich growth of a GaN(000$\bar{1}$) layer. (f) Corresponding bird's eye view scanning electron micrograph acquired after the N-rich growth process.

growth conditions is caused by the formation of a wealth of $\{1\bar{1}0\bar{n}\}_{n\geqslant 2}$ semipolar facets. These results demonstrate that during GaN(000$\bar{1}$) growth in PA-MBE, a decrease in the Ga chemical potential at the surface triggers a shape transition that results in the formation of well-defined semipolar facets. These facets are similar but not identical to those obtained after thermal decomposition in vacuum. In the context of a surface morphology controlled by the Ga chemical potential, the variety of semipolar facets observed here could be explained by a freezing of the system at intermediate local energy minimums due to the large diffusion barriers experienced by Ga and N adatoms in the absence of a Ga wetting layer [46].

IV. DISCUSSION

The temperature-induced faceting of N-polar GaN nanowires and planar layers found in this work was neither predicted by theoretical calculations [17] nor seen in the kinetic Wulff constructions reported in Refs. [47] and [48]. In the case of GaN nanowires, the reshaping occurs after a delay time and goes through the formation of high- to low-indexed $\{1\bar{1}0\bar{n}\}_{n\geqslant 2}$ semipolar facets. Under vacuum exposure, the final nanowire shape is characterized by the formation of {1$\bar{1}$0$\bar{2}$} facets at the nanowire tips. Alternatively, {1$\bar{1}$0$\bar{8}$} top-facets can be stabilized for several minutes using N exposure at a substrate temperature below 880 °C. The temperature dependence of the characteristic reshaping time reveals that there are energy barriers higher than 3 eV to overcome, in order to reach the final nanowire shape. In the vacuum exposure case, it is remarkable that the actual value of the energy barrier depends on the background concentration of active N inside the chamber. This observation is reminiscent of the reported increase in the apparent energy barrier for GaN(0001) thermal decomposition under N exposure [49]. On this basis, the stabilization of {1$\bar{1}$0$\bar{8}$} top-facets obtained under N but not vacuum exposure is assigned to a kinetic freezing of the system in an intermediate minimum along the reshaping path toward the {1$\bar{1}$0$\bar{2}$} top-facets. The freezing would be caused by an increase of the energy barrier between the {1$\bar{1}$0$\bar{8}$} and {1$\bar{1}$0$\bar{2}$} configurations in the presence of active N adatoms. Low substrate temperature and high N fluxes should then be preferred to increase the lifetime of the transient {1$\bar{1}$0$\bar{8}$} facets, although these conditions would

also increase the delay time. By extrapolation, it cannot be excluded either that $\{1\bar{1}02\}$ top-facets also constitute an intermediate step along the reshaping path, in which the system kinetically freezes under vacuum exposure for the temperatures and exposure times explored in this study.

In this framework, the reshaping of GaN nanowires could be explained in terms of a lower energy barrier for thermally decomposing GaN$(1\bar{1}0\bar{n})$ than GaN$(000\bar{1})$ [50,51]. However, such a simple scenario does not provide an explanation for the delay time observed prior to the reshaping, during which GaN nanowires decompose while preserving their original shape. Instead, we propose that the nanowire reshaping process is triggered by a change in the Ga chemical potential, as observed in the case of planar layers. This change could induce the reshaping due to either (i) the direct dependence of the surface energy on the chemical potential [17] (thermodynamic control), or (ii) variations in the energy barriers for the thermal decomposition of different facets (kinetic control). Under this assumption, regardless of whether the reshaping is thermodynamically or kinetically driven, the delay time would always represent the average time required to vary the Ga chemical potential at the nanowire tips.

The lag in the change in the Ga chemical potential after initiating the thermal decomposition process of GaN nanowire ensembles could be due to the enhanced decomposition rate of GaN in the vicinity of the extended defects created at the nanowire coalescence joints as well as in the parasitic layer formed in between nanowires (when they are prepared on AlN-buffered Si). Since the Ga adatoms resulting from the thermal decomposition of GaN have a certain surface residence time before being desorbed [23], the enhanced decomposition rate at structural defects could feed a reservoir of Ga adatoms free to diffuse toward the nanowire tips [52,53]. Only once this reservoir runs empty, the Ga chemical potential at the nanowire tips could drop below the threshold value that triggers the shape transformation. This picture would also explain the steady increase of the delay time with the duration of GaN growth prior to nanowire reshaping [Fig. 3(c)], namely, the longer the growth time, the larger the Ga adatom reservoir. Interestingly, since Ga diffusion in nanowire ensembles partially occurs through the exchange of adatoms between adjacent nanowires [53]—a collective effect that quantitatively varies from nanowire to nanowire due to their random neighborhoods—significant fluctuations in the Ga chemical potential are expected within the ensemble. Consequently, the established connection between the reshaping process and the Ga chemical potential at the nanowire tips provides explanations for both the dispersion observed in the shape of the nanowire tips after the reshaping process and the synchronized shape transformation of nanowires separated by several hundred microns.

V. SUMMARY AND CONCLUSIONS

We have shown that thermal decomposition of as-grown N-polar GaN nanowires at low pressure and in the 800–910 °C range can result in the formation of $\{1\bar{1}02\}$ and $\{1\bar{1}0\bar{8}\}$ semipolar top-facets depending on whether the process takes place under vacuum or N exposure, respectively. The reshaping is reversible; i.e., the original $(000\bar{1})$ top-facets of as-grown nanowires can be recovered during subsequent GaN growth. Hence, thermal decomposition enables an on-demand control on the shape of GaN nanowires.

The reshaping process can be monitored *in vivo* using RHEED by tracking the formation and subsequent evolution of chevrons in the diffraction pattern. The *in situ* and *ex situ* analysis of the process reveals the existence of a delay time prior to the actual shape transformation which is correlated with a transient in the GaN decomposition rate measured by QMS. Once the actual reshaping sets in, it proceeds through the formation of high-index semipolar facets ($\{1\bar{1}0\bar{n}\}$) until reaching the final $\{1\bar{1}02\}$ facets. The reshaping requires overcoming several energy barriers higher than 3 eV, which can result in a freezing of the system in intermediate energy minimums, such as $\{1\bar{1}0\bar{8}\}$ facets in the case of N exposure.

Since the formation of semipolar facets is also observed in planar layers, we conclude that the reshaping process is not related to the peculiar nanowire geometry. We propose that the reshaping process of GaN nanowires, which could be driven by either thermodynamic or kinetic effects, is triggered by a change in the Ga chemical potential at the nanowire tips which should drop below a certain threshold value to initiate the shape transformation. According to this picture, the delay time preceding the nanowire reshaping is attributed to a lag in the change of the chemical potential at the nanowire tips induced by the existence of a Ga reservoir fed by the fast decomposition of GaN defective regions present in the samples.

Thermal decomposition of GaN has been reported harmless for its optical properties [26]. Hence, this unprecedented ability to transform the shape of GaN nanowires may find applications for the fabrication of semipolar nanowire axial heterostructures benefiting from a reduced internal electric field [54] as compared to their polar counterparts. In a different context, forming a pencil-like top-facet could ease the field effect ionization of the nanowire tip for atom probe tomography analyses and be of use for the fabrication of advanced nanowire-based probing tips for atomic force microscopy experiments combined with local optical excitations. At last, these results are also of interest for the incipient top-down fabrication of different types of group-III nitride nanostructures by selective area sublimation [55–57].

ACKNOWLEDGMENTS

We thank Katrin Morgenroth for her support during the preparation of the samples as well as for her dedicated maintenance of the molecular beam epitaxy system together with Carsten Stemmler and Michael Höricke. We thank Anne-Kathrin Bluhm for the acquisition of scanning electron micrographs. Furthermore, we thank Caroline Chèze for a critical reading of the manuscript. Funding from both the Bundesministerium für Bildung und Forschung through Project No. FKZ:13N13662 and the Leibniz-Gemeinschaft under Grant No. SAW-2013-PDI-2 is gratefully acknowledged. S.F.-G. acknowledges the partial financial support received through the Spanish program Ramón y Cajal (cofinanced by the European Social Fund) under Grant No. RYC-2016-19509 from Ministerio de Ciencia, Innovación y Universidades.

[1] V. Bermudez, Surf. Sci. Rep. **72**, 147 (2017).

[2] P. Waltereit, O. Brandt, A. Trampert, H. T. Grahn, J. Menniger, M. Ramsteiner, M. Reiche, and K. H. Ploog, Nature (London) **406**, 865 (2000).

[3] S. Fernández-Garrido, J. Lähnemann, C. Hauswald, M. Korytov, M. Albrecht, C. Chèze, C. Skierbiszewski, and O. Brandt, Phys. Rev. Applied **6**, 034017 (2016).

[4] F. Scholz, Semicond. Sci. Technol. **27**, 024002 (2012).

[5] A. Kikuchi, M. Kawai, M. Tada, and K. Kishino, Jpn. J. Appl. Phys. **43**, L1524 (2004).

[6] J. Renard, R. Songmuang, G. Tourbot, C. Bougerol, B. Daudin, and B. Gayral, Phys. Rev. B **80**, 121305 (2009).

[7] R. Koester, J.-S. Hwang, D. Salomon, X. Chen, C. Bougerol, J.-P. Barnes, D. L. S. Dang, L. Rigutti, A. de Luna Bugallo, G. Jacopin, M. Tchernycheva, C. Durand, and J. Eymery, Nano Lett. **11**, 4839 (2011).

[8] M. Hetzl, J. Winnerl, L. Francaviglia, M. Kraut, M. Doblinger, S. Matich, A. Fontcuberta i Morral, and M. Stutzmann, Nanoscale **9**, 7179 (2017).

[9] Y. Zhang, J. Wu, M. Aagesen, and H. Liu, J. Phys. D: Appl. Phys. **48**, 463001 (2015).

[10] J. Zúñiga-Pérez, V. Consonni, L. Lymperakis, X. Kong, A. Trampert, S. Fernández-Garrido, O. Brandt, H. Renevier, S. Keller, K. Hestroffer, M. R. Wagner, J. S. Reparaz, F. Akyol, S. Rajan, S. Rennesson, T. Palacios, and G. Feuillet, Appl. Phys. Rev. **3**, 041303 (2016).

[11] L. Largeau, D. L. Dheeraj, M. Tchernycheva, G. E. Cirlin, and J. C. Harmand, Nanotechnology **19**, 155704 (2008).

[12] A. Urban, J. Malindretos, J.-H. Klein-Wiele, P. Simon, and A. Rizzi, New J. Phys. **15**, 053045 (2013).

[13] X. Kong, H. Li, S. Albert, A. Bengoechea-Encabo, M. A. Sanchez-Garcia, E. Calleja, C. Draxl, and A. Trampert, Nanotechnology **27**, 065705 (2016).

[14] K. Hestroffer, C. Leclere, C. Bougerol, H. Renevier, and B. Daudin, Phys. Rev. B **84**, 245302 (2011).

[15] A. Minj, A. Cros, N. Garro, J. Colchero, T. Auzelle, and B. Daudin, Nano Lett. **15**, 6770 (2015).

[16] M. D. Brubaker, S. M. Duff, T. E. Harvey, P. T. Blanchard, A. Roshko, A. W. Sanders, N. A. Sanford, and K. A. Bertness, Cryst. Growth Des. **16**, 596 (2016).

[17] H. Li, L. Geelhaar, H. Riechert, and C. Draxl, Phys. Rev. Lett. **115**, 085503 (2015).

[18] B. Heying, R. Averbeck, L. F. Chen, E. Haus, H. Riechert, and J. S. Speck, J. Appl. Phys. **88**, 1855 (2000).

[19] V. Consonni, Phys. Status Solidi RRL **7**, 699 (2013).

[20] L. Largeau, E. Galopin, N. Gogneau, L. Travers, F. Glas, and J.-C. Harmand, Cryst. Growth Des. **12**, 2724 (2012).

[21] T. Suzuki and Y. Hirabayashi, Jpn. J. Appl. Phys. **32**, L610 (1993).

[22] R. Groh, G. Gerey, L. Bartha, and J. I. Pankove, Phys. Status Solidi A **26**, 353 (1974).

[23] S. Fernández-Garrido, G. Koblmüller, E. Calleja, and J. S. Speck, J. Appl. Phys. **104**, 033541 (2008).

[24] G. Koblmüller, R. Averbeck, H. Riechert, and P. Pongratz, Phys. Rev. B **69**, 035325 (2004).

[25] S. Fernández-Garrido, J. K. Zettler, L. Geelhaar, and O. Brandt, Nano Lett. **15**, 1930 (2015).

[26] J. K. Zettler, P. Corfdir, C. Hauswald, E. Luna, U. Jahn, T. Flissikowski, E. Schmidt, C. Ronning, A. Trampert, L. Geelhaar, H. T. Grahn, O. Brandt, and S. Fernández-Garrido, Nano Lett. **16**, 973 (2016).

[27] C. Chèze, M. Sawicka, M. Siekacz, H. Turski, G. Cywiński, J. Smalc-Koziorowska, J. L. Weyher, M. Kryśko, B. Łucznik, M. Boćkowski, and C. Skierbiszewski, Appl. Phys. Lett. **103**, 071601 (2013).

[28] T. Auzelle, B. Haas, A. Minj, C. Bougerol, J.-L. Rouvière, A. Cros, J. Colchero, and B. Daudin, J. Appl. Phys. **117**, 245303 (2015).

[29] T. Stoica, E. Sutter, R. J. Meijers, R. K. Debnath, R. Calarco, H. Lüth, and D. Grützmacher, Small **4**, 751 (2008).

[30] T. Hanada, B.-H. Koo, H. Totsuka, and T. Yao, Phys. Rev. B **64**, 165307 (2001).

[31] D. Pashley, J. Neave, and B. Joyce, Surf. Sci. **476**, 35 (2001).

[32] J. Lee, D. Schuh, M. Bichler, and G. Abstreiter, Appl. Surf. Sci. **228**, 306 (2004).

[33] I. Ayahiko and P. I. Cohen, *Reflection High-Energy Electron Diffraction* (Cambridge University Press, Cambridge, UK, 2004).

[34] H. R. Gutiérrez, M. A. Cotta, and M. M. G. de Carvalho, Appl. Phys. Lett. **79**, 3854 (2001).

[35] E. Placidi, A. D. Pia, and F. Arciprete, Appl. Phys. Lett. **94**, 021901 (2009).

[36] A. Feltrin and A. Freundlich, J. Cryst. Growth **301–302**, 38 (2007).

[37] N. Ohshima, Y. Koide, K. Itoh, S. Zaima, and Y. Yasuda, Appl. Phys. Lett. **57**, 2434 (1990).

[38] T. Kudo, T. Inoue, T. Kita, and O. Wada, J. Appl. Phys. **104**, 074305 (2008).

[39] C. Gaire, F. Tang, and G.-C. Wang, Thin Solid Films **517**, 4509 (2009).

[40] M. Krawczyk, L. Zommer, A. Jablonski, I. Grzegory, and M. Bockowski, Surf. Sci. **566–568**, 1234 (2004).

[41] E. Galopin, L. Largeau, G. Patriarche, L. Travers, F. Glas, and J. C. Harmand, Nanotechnology **22**, 245606 (2011).

[42] V. M. Kaganer, S. Fernández-Garrido, P. Dogan, K. K. Sabelfeld, and O. Brandt, Nano Lett. **16**, 3717 (2016).

[43] B. Jenichen, O. Brandt, C. Pfüller, P. Dogan, M. Knelangen, and A. Trampert, Nanotechnology **22**, 295714 (2011).

[44] K. Grossklaus, A. Banerjee, S. Jahangir, P. Bhattacharya, and J. Millunchick, J. Cryst. Growth **371**, 142 (2013).

[45] H. Okumura, B. M. McSkimming, T. Huault, C. Chaix, and J. S. Speck, Appl. Phys. Lett. **104**, 012111 (2014).

[46] T. Zywietz, J. Neugebauer, and M. Scheffler, Appl. Phys. Lett. **73**, 487 (1998).

[47] Q. Sun, C. D. Yerino, B. Leung, J. Han, and M. E. Coltrin, J. Appl. Phys. **110**, 053517 (2011).

[48] B. N. Bryant, A. Hirai, E. C. Young, S. Nakamura, and J. S. Speck, J. Cryst. Growth **369**, 14 (2013).

[49] B. M. McSkimming, C. Chaix, and J. S. Speck, J. Vac. Sci. Technol., A **33**, 05E128 (2015).

[50] R. C. Snyder and M. F. Doherty, AIChE J. **53**, 1337 (2007).

[51] M. R. Singh, N. Nere, H.-H. Tung, S. Mukherjee, S. Bordawekar, and D. Ramkrishna, Cryst. Growth Des. **14**, 5647 (2014).

[52] V. Consonni, V. G. Dubrovskii, A. Trampert, L. Geelhaar, and H. Riechert, Phys. Rev. B **85**, 155313 (2012).

[53] K. K. Sabelfeld, V. M. Kaganer, F. Limbach, P. Dogan, O. Brandt, L. Geelhaar, and H. Riechert, Appl. Phys. Lett. **103**, 133105 (2013).

[54] A. E. Romanov, T. J. Baker, S. Nakamura, J. S. Speck, and E. U. Group, J. Appl. Phys. **100**, 023522 (2006).

[55] K. Ogawa, R. Hachiya, T. Mizutani, S. Ishijima, and A. Kikuchi, Phys. Status Solidi A **214**, 1600613 (2016).

[56] B. Damilano, S. Vézian, J. Brault, B. Alloing, and J. Massies, Nano Lett. **16**, 1863 (2016).

[57] B. Damilano, S. Vézian, and J. Massies, Opt. Express **25**, 33243 (2017).